White Rose Research Online

eprints@whiterose.ac.uk
https://eprints.whiterose.ac.uk
Universities of Leeds, Sheffield and York

Deposited via The University of York.

White Rose Research Online URL for this paper:
https://eprints.whiterose.ac.uk/id/eprint/189248/

Version: Published Version

Article:
Si, Jikai, Feng, Can, Nie, Rui et al. (2021) A novel high torque density six-phase axial-flux permanent magnet synchronous motor with 60° phase-belt toroidal winding configuration. IET Electric Power Applications. pp. 41-54. ISSN: 1751-8679

https://doi.org/10.1049/elp2.12133

Reuse
This article is distributed under the terms of the Creative Commons Attribution (CC BY) licence. This licence allows you to distribute, remix, tweak, and build upon the work, even commercially, as long as you credit the authors for the original work. More information and the full terms of the licence here: https://creativecommons.org/licenses/

Takedown
If you consider content in White Rose Research Online to be in breach of UK law, please notify us by emailing eprints@whiterose.ac.uk including the URL of the record and the reason for the withdrawal request.

UNIVERSITY OF LEEDS
University of Sheffield
UNIVERSITY of York

Received: 8 June 2021 | Revised: 30 July 2021 | Accepted: 31 August 2021

DOI: 10.1049/elp2.12133

IET Electric Power Applications

The Institution of Engineering and Technology WILEY

ORIGINAL RESEARCH PAPER

A novel high torque density six-phase axial-flux permanent magnet synchronous motor with 60° phase-belt toroidal winding configuration

Jikai Si[1] | Can Feng[1] | Rui Nie[1] | Yihua Hu[2] | Yingsheng Li[3]

[1]College of Electric Engineering, Zhengzhou University, Zhengzhou, Henan, China

[2]Department of Electronic Engineering, University of York, York, UK

[3]Zhengzhou Runhua Intelligent Equipment Co., Ltd, Zhengzhou, China

Correspondence

Rui Nie, College of Electric Engineering, Zhengzhou University, Zhengzhou, Henan 450001, China.
Email: nierui@zzu.edu.cn

Funding information

Natural Science Foundation of China under grant, Grant/Award Number: 51777060; China Postdoctoral Science Foundation, Grant/Award Number: 2020M682342; Major Special Project for Collaborative Innovation in Zhengzhou, Grant/Award Number: 20XTZX12023

Abstract

The three-phase permanent magnet synchronous motor (three-phase PMSM) has gained much popularity in many applications due to its various advantages. In addition, due to the good fault tolerance, simple inverter circuit structure and high torque density, the six-phase PMSM has better prospects than three-phase PMSM in biomedical devices, electric vehicles and other fields with high reliability requirements. In this study, a six-phase axial-flux PMSM inherently without cogging torque is proposed to improve torque density, which equips the 60° phase-belt toroidal winding (60°TW) and slotless stator core. Based on the same effective volume, permanent magnet material, power grade and the other major motor parameters, two six-phase PMSMs with 30° phase-belt toroidal winding (30°TW) and 60°TW are designed, respectively. The armature reaction field, air gap magnetic density, back-electromotive force, output torque, loss characteristic and torque-speed characteristic are compared by using three-dimensional (3D) finite-element models in detail. Finally, the experimental test is carried out using the prototype of three-phase PMSM with 120° phase-belt toroidal winding. The experimental results indirectly verify the feasibility of 60° phase-belt toroidal winding and correctness of 3D FEM. The 3D FEM analysis results are presented to show that torque density of the proposed six-phase PMSM with 60°TW is improved in comparison to the six-phase PMSM with 30°TW.

Index Terms—60° phase-belt toroidal winding, axial flux, six-phase permanent magnet synchronous motor, torque density

KEYWORDS

electrochemical analysis, finite element analysis, losses, machine windings, permanent magnet motors

1 | INTRODUCTION

With the rapid development of power electronic technology, microelectronic technology and automatic control theory, permanent magnet synchronous motors have been widely applied in electric vehicles, biped robots and other fields due to low torque ripple, high efficiency, high power factor and so on [1–3]. Moreover, high torque density is urgently required for various applications such as biomedical devices and electric vehicles to obtain higher efficiency drive [4, 5]. Thus, achieving higher torque density is always one of the emphases of research.

To further improve the torque density of the motor, many scholars have carried out a lot of related research studies, such as changing the structure of motor, altering the cooling way, injecting high harmonic current and so on. In [6, 7], double stator electric machine and alternate polarities circumferentially magnetised permanent magnet are proposed to improve torque density. The direct liquid cooling method which could sustain higher torque is suggested in [8]. In [9, 10], it can be found that injecting third and high harmonic current can improve output torque. However, altering motor structure and cooling way change the shape of the motor and make it harder to manufacture the motor.

This is an open access article under the terms of the Creative Commons Attribution License, which permits use, distribution and reproduction in any medium, provided the original work is properly cited.

© 2021 The Authors. *IET Electric Power Applications* published by John Wiley & Sons Ltd on behalf of The Institution of Engineering and Technology.

Moreover, injecting high harmonic current has a higher requirement for the drive system.

In addition to the motor structure and cooling mode, the winding configuration also plays a key role in obtaining high torque density for PMSM [11]. Hence, people try to improve the torque density by modifying the winding layouts which is simpler and more convenient. Because of the simple manufacture feature, integer slot windings are very common for the conventional PMSM [12]. Meanwhile, fractional-slot concentrated-winding has aroused interest over the past few years due to its short end turns and high power density [13]. However, when the axial length of the motor is limited, overlapping distributed windings will lead to long end-winding while concentrated windings will lead to low winding factors, which will hinder the improvement of torque density [14, 15]. Therefore, toroidal winding is proposed to suit the machine whose axial length is limited and to realise structures that cannot be realised by traditional windings [16].

In recent years, the PMSM equipped with toroidal winding has been widely studied. In [17], an integer-slot toroidal-winding double PM-rotor direct drive permanent magnet (DDPM) machine is proposed to obtain better torque performance. Meanwhile, a fractional-slot radial-flux permanent magnet motor with toroidal winding is proposed in [18], and the results show that employing toroidal winding can increase the torque within a certain range. In addition, a machine that equips 120° phase-belt toroidal winding is proposed in [19] and compared with motor employed traditional toroidal winding. It can be seen that the proposed motor has higher torque density, which proves that proposed toroidal winding has a better torque characteristic than that of traditional toroidal winding. However, as shown in Figure 1, the three-phase toroidal winding motor proposed in [19] has a large second harmonic in the armature reaction field. Large second harmonic leads to the asymmetric armature reaction field. This will make the main magnetic field asymmetric, which results in local high temperature of the rotor and intensified vibration. Thus, in order to improve the armature magnetic field and the torque density of the motor, a radial-flux six-phase winding motor with 60° phase-belt toroidal winding is proposed in [20]. It can be found that the output torque of a machine with 60° phase-belt toroidal winding configuration is larger than that of a 30° phase-belt toroidal winding PMSM. In general, a six-phase machine has more symmetrical armature magnetic field and better performance than those of a three-phase machine. However, the utilisation ratio of toroidal winding of the proposed motor in [20] is low because of its single rotor structure. Furthermore, achieving high torque density with light and thin structure is difficult for a radial permanent magnet motor [21]. Therefore, the axial-flux permanent magnet machine, especially the double-rotor toroidal winding motor is getting more attention because the two rotors can be placed at an optimum torque diameter [18]. Meanwhile, the axial-flux motor also has advantages such as short axial length, high torque density and various stator structures [22, 23]. From the above analysis, it can be found that the research study on improving the torque density mainly focusses on the three-phase PMSM, but there are few studies on the six-phase PMSM with toroidal winding.

In this study, according to the advantages of axial-flux and toroidal winding, a six-phase axial-flux PMSM with 60° phase-belt toroidal winding configuration (60°TW-SPMSM) is proposed. The no-load back-electromotive force (EMF), armature reaction field, air gap magnetic density, torque performance and loss characteristic of the proposed motor and the axial-flux six-phase PMSM with 30° phase-belt toroidal winding (30°TW-SPMSM) are compared. First, the motor structure is introduced, and its operation principle is reported. Second, the design of the proposed motor is described. Then, the influences of different load conditions on the motor performances are studied. Finally, it proves that the toroidal winding can produce rotating magnetic field by measurements on the prototype machine of the three-phase PMSM with 120° phase-belt toroidal winding (120°TW-PMSM). The results verify the consistency of three-dimensional (3D) finite-element analysis results and experimental results.

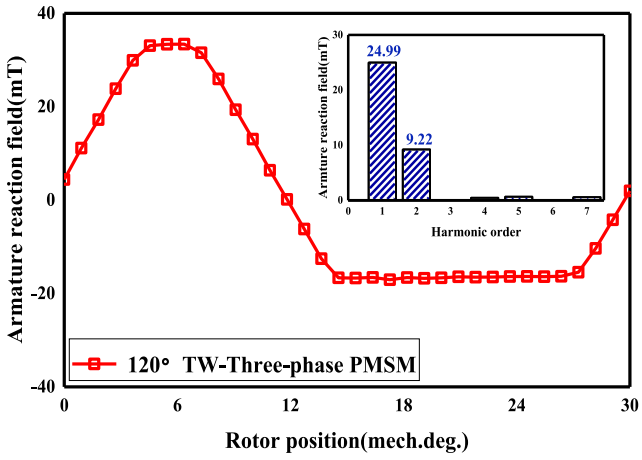

FIGURE 1 Armature reaction field and harmonic order of the three-phase PMSM with 120° phase-belt toroidal winding

2 | STRUCTURE AND OPERATION PRINCIPLE OF 60°TW-SPMSM

2.1 | Structure

The structure of 60°TW-SPMSM is shown in Figure 2(a), which employs the outer rotor core and inner stator core. Moreover, the rotor on both sides of the proposed motor are symmetrical. It can be clearly seen that the air gap between the stator and rotor of the motor is a plane perpendicular to the rotating shaft of the motor. Figure 2(b) is the minimum unit of the proposed 60°TW-SPMSM, and the arrows show the direction of current at a given time. It can be noted that the permanent magnets of the proposed motor are symmetrically distributed along the axial direction. The same axial permanent magnet has the same polarity, N-N or S-S.

In order to illustrate the structural characteristics of 60° TW-SPMSM and 30°TW-SPMSM, the simplified views of winding connection of two six-phase machines are shown in Figure 3. Figure 3a shows the winding configuration of

60°TW-SPMSM, and Figure 3b shows the winding configuration of 30°TW-SPMSM. It can be seen that the difference between each winding of 60°TW-SPMSM is 60°. Thus, the winding form is named as 60° phase-belt toroidal winding (60°TW).

2.2 | Mechanism analysis

Each phase of the proposed motor is excited by a six-phase sinusoidal alternating current. Figure 4 shows the waveform of the incoming currents.

According to the current distribution of the stator windings at different time in a cycle and right-hand screw rule, the distribution of magnetic fields at each time are described in Figure 5. The current direction of the six graphs in Figure 5 corresponds to the current direction of the six moments in Figure 4. The analysis results of magnetic field show that the proposed six-phase PMSM forms a pair of poles per three phase. In addition, two rotating magnetic fields with the identical direction and rotational speed are generated on both sides of the stator core when the six-phase symmetrical currents flow into the 60°TW-SPMSM. Therefore, the two rotors rotate synchronously with the interaction of the permanent magnetic field and armature magnetic field.

3 | DESIGN OF THE MOTORS

The two rotors of the proposed motor are symmetrical in the centre plane of the disc stator core, so any side divided by the symmetry plane of the stator core can be taken as the analysis object, that is, the motor can be designed with a single stator-single rotor structure.

Average electromagnetic power of 60°TW-SPMSM can be obtained by back electromotive force and current as shown in the first formula which can be obtained in [24]:

$$P_{\text{out}} = \eta \frac{m}{T} \int_0^T e(t) i(t) \mathrm{d}t = \eta m K_{\text{P}} E_{\text{Pk}} I_{\text{Pk}} \tag{1}$$

where η is the motor efficiency, m is the phase number of the motor, $e(t)$ is the instantaneous value of the opposite electromotive force, $i(t)$ is the instantaneous value of the phase current, T is a period of the EMF, and K_{P} is the power

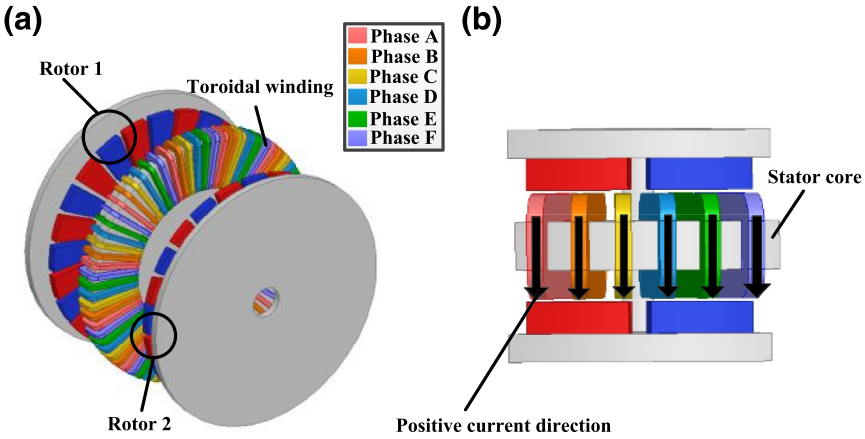

FIGURE 2 Topology of the proposed six-phase PMSM. (a) structure block. (b) minimum unit model

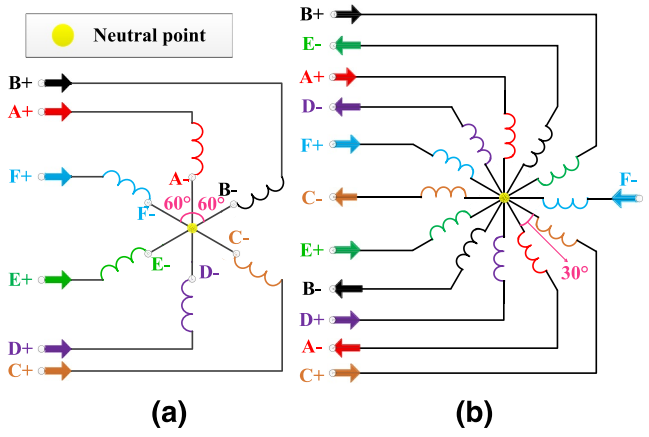

FIGURE 3 Winding connection of two six-phase PMSMs. (a) 60°TW-SPMSM. (b) 30°TW-SPMSM

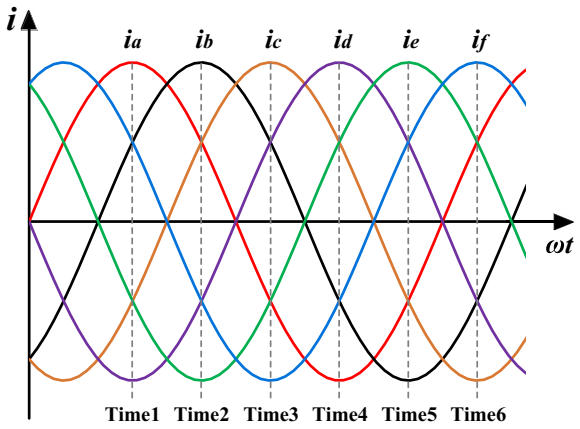

FIGURE 4 Phase currents at different time

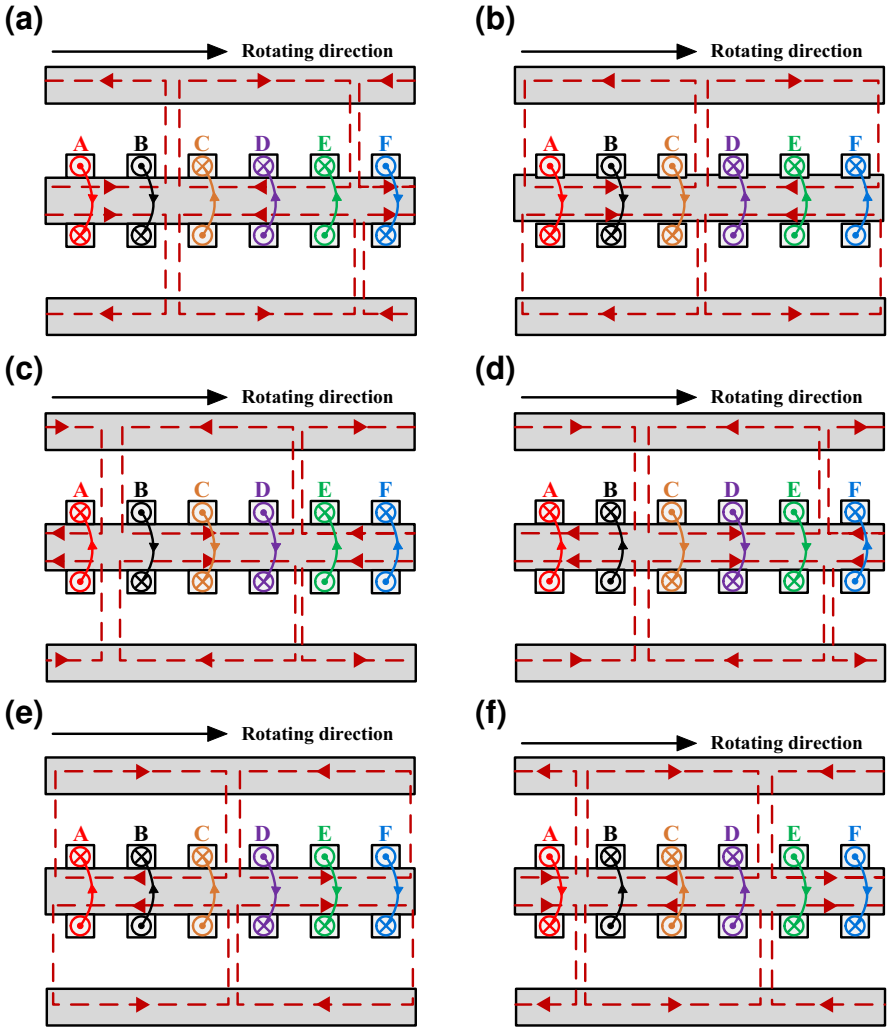

FIGURE 5 Magnetic field distribution at each time. (a) Time 1. (b) Time 2. (c) Time 3. (d) Time 4. (e) Time 5. (f) Time 6

waveform coefficient considering the electromotive force and current waveform.

The peak value of the phase EMF can be found in [25] and expressed by

$$E_{\mathrm{Pk}} = \frac{1}{2} K_{\mathrm{e}} N_{\mathrm{Ph}} B_{\mathrm{g}} f \left(1 - K_{\mathrm{r}}^2\right) D_{\mathrm{o}}^2 / p \tag{2}$$

where K_{e} is the EMF factor including the winding distribution factor and the ratio between the total airgap area and the area spanned by the salient poles, N_{Ph} is the number of turns of phase winding, p is the number of pole pairs, f is the rated frequency, Kr is the ratio of inner diameter to outer diameter of the motor and D_{o} is the outer diameter of the stator core.

The electric load A of two motors can be expressed as follows:

$$A = m N_{\mathrm{Ph}} \frac{I_{\mathrm{rms}}}{\pi D_{\mathrm{a}}} \tag{3}$$

where I_{rms} is the effective value of phase current, D_{a} is the average inner and outer diameter of the stator core. Since the current flows from the same side of the proposed motor winding, the number of conductors is half of the number of turns of the traditional motor. So the coefficient of Equation (3) is half of the formula in [25].

The general expression of the phase current peak is different from the formula in [25] due to the change of A, which can be expressed by

$$I_{\mathrm{Pk}} = \frac{\sqrt{2}\pi A D_{\mathrm{a}}}{m N_{\mathrm{ph}}} = \frac{\sqrt{2}\pi A (1 + K_{\mathrm{r}}) D_{\mathrm{o}}}{2 m N_{\mathrm{Ph}}} \tag{4}$$

Based on Equations (1), (2) and (4), the expressions of output power and torque of the motor can be obtained in [25] which only have different coefficients:

$$P_{\mathrm{out}} = \frac{\sqrt{2}}{4} \pi \eta K_{\mathrm{P}} K_{\mathrm{e}} B_{\mathrm{g}} A f \left(1 - K_{\mathrm{r}}^2\right)(1 + K_{\mathrm{r}}) D_{\mathrm{o}}^3 / p \tag{5}$$

$$T_{\mathrm{out}} = \frac{\sqrt{2}}{8} \eta K_{\mathrm{P}} K_{\mathrm{e}} B_{\mathrm{g}} A \left(1 - K_{\mathrm{r}}^2\right)(1 + K_{\mathrm{r}}) D_{\mathrm{o}}^3 \tag{6}$$

For permanent magnets of the proposed motor, the demagnetisation curve is linear to a certain extent, and the

B_g/B_r is 0.5 at the maximum magnetic energy product, and the remanence of N48SH is about 1.4 T. So the air gap flux density is about 0.7 T [24]. (In page seven of response paper.)

From the above, the winding thickness W_{C_u} can be calculated by [24]:

$$\frac{B_g}{B_r} = \frac{L_m}{W_{C_u} + g + L_m} = 0.5 \tag{7}$$

where L_m is the axial thickness of the permanent magnet.

When torque and torque density are both considered, the optimal Kr value is between 0.6 and 0.7. Therefore, the ratio Kr of inner and outer diameters of the stator yoke studied in this work is 0.65.

For verification, an axial-flux six-phase PMSM with 60° phase-belt toroidal winding model is designed and compared with the six-phase motor which employs 30° phase-belt toroidal winding. In order to ensure the motors are compared under the same standard and the reliability of the simulation comparison results, the design needs to meet the following criteria:

(i) The two motors have the same outer diameter of the rotor, inner diameter of the stator and air-gap length to ensure the same effective volumes.
(ii) The two motors have the same amount of permanent magnets, pole arc coefficient, properties of permanent magnet materials and magnetising height of permanent magnet.
(iii) The number of conductors and the winding diameter within one slot of two motors are the same.

According to the above criteria, the primary parameters of the proposed motor (60°TW-SPMSM) and six-phase motor with 30° phase-belt toroidal winding (30°TW-SPMSM) are presented in Table 1.

4 | FINITE-ELEMENT ANALYSIS AND COMPARISON

Finite-element analysis is conducted in the two motors to calculate the back-EMF, magnetic density distribution and air-gap magnetic density waveforms of the motors under the no-load condition. In addition, the armature reaction field, output torque, torque-speed characteristic and efficiency of two motors under load condition are analysed in particular. The value of the peak rated current is 14.44 A while the rated frequency is 80 Hz.

4.1 | Back-EMF

The no-load back-EMF of the slotless axial-flux PMSM with toroidal winding depends on the outer and inner radius of the stator core, the number of turns per phase, the air-gap magnetic flux density, the width of the coil and so on [26]. In addition, the vector diagram of phase no-load back-EMF of 60°TW-SPMSM and 30°TW-SPMSM is shown in Figure 6.

The no-load back-EMF of one coil of the slotless axial-flux PMSM can be calculated by [26].

$$E_c = \frac{2}{\pi}\Omega B_g \int_{R_i}^{R_0} \frac{\sin\left(\frac{1+N_c}{N_c}\cdot\frac{h\cdot p}{r}\right)}{\sin\left(\frac{h\cdot p}{rN_c}\right)} r\,dr \tag{8}$$

where, R_i is the inner radius of the stator core, R_o is the outer radius of the stator core, Ω is the angular velocity of motor rotating machinery, B_g is the fundamental amplitude of the air-gap magnetic flux density, N_c is the number of turns of the coil, h is the width of the coil, p is the number of pole pairs, and r is the radius length of the radial length of the coil.

Compared with 30°TW-SPMSM, the turns of per coil and the width of coils of 60°TW-SPMSM are doubled. Therefore, in order to simplify the calculation, this study assumes that the single coil of 60°TW-SPMSM is composed of two single coils of the 30°TW-SPMSM. According to Equation (8) and above

TABLE 1 Primary parameters of the proposed motors

Items	60°TW-SPMSM	30°TW-SPMSM
Rated speed (RPM)	400	400
Rated current (A)	10	10
Rated voltage (V)	40	40
Rated power (kW)	2.4	2.4
Number of phase	6	6
Coil number	72	144
Turns of per coil	24	12
Pole number	24	24
Outer diameter of rotor (mm)	254	254
Inner diameter of rotor (mm)	30	30
Outer diameter of stator (mm)	240	240
Inner diameter of stator (mm)	156	156
Air gap (mm)	1	1
Permanent magnet thickness (mm)	8	8

Abbreviations: 30°TW-SPMSM, 30° phase-belt toroidal winding; 60°TW-SPMSM, 60° phase-belt toroidal winding configuration.

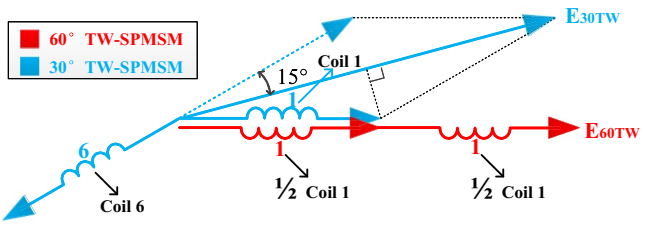

FIGURE 6 Vector diagram of phase no-load back-electromotive force of 1/12 model of two motors

analysis, the no-load back-EMF of one coil of 30°TW-SPMSM is equal to the no-load back-EMF of half coil of 60°TW-SPMSM.

According to the phase-belt of the proposed motor and Figure 6, the no-load back-EMF of the 1/12 model of 60°TW-SPMSM can be expressed as follows:

$$E_{60\mathrm{Tw}} = 2E_{\mathrm{c}} = \frac{4}{\pi}\Omega B_{\mathrm{g}} \int_{R_{\mathrm{i}}}^{R_0} \frac{\sin\left(\frac{1+N_{\mathrm{c}}}{N_{\mathrm{c}}} \cdot \frac{h \cdot p}{r}\right)}{\sin\left(\frac{h \cdot p}{rN_{\mathrm{c}}}\right)} r\mathrm{d}r \tag{9}$$

According to Figure 6, the no-load back-EMF of 1/12 model of 30°TW-SPMSM can be expressed as follows:

$$\begin{aligned} E_{30\mathrm{Tw}} &= 2E_{\mathrm{c}} \cos\frac{\pi}{12} \\ &= \frac{(\sqrt{6}+\sqrt{2})}{\pi}\Omega B_{\mathrm{g}} \int_{R_{\mathrm{i}}}^{R_0} \frac{\sin\left(\frac{1+N_{\mathrm{c}}}{N_{\mathrm{c}}} \cdot \frac{h \cdot p}{r}\right)}{\sin\left(\frac{h \cdot p}{rN_{\mathrm{c}}}\right)} r\mathrm{d}r \end{aligned} \tag{10}$$

If the known parameters are brought into Equations (9) and (10), it can be concluded that the no-load back-EMF of 60°TW-SPMSM is 3.53% higher than that of 30°TW-SPMSM.

The no-load back-EMFs of 60°TW-SPMSM and 30°TW-SPMSM at rated speed (400 rpm) are shown in Figure 7. It can be found that the back-EMF peak of 60°TW-SPMSM is 51.29 V while that of 30°TW-SPMSM is 50.89 V. Figure 7 and Table 2 show the harmonic order of back-EMF.

According to Fourier analysis, the amplitudes of fundamental component of back-EMF of 60°TW-SPMSM and 30° TW-SPMSM are 56.08 and 54.13 V, respectively. It can be found that the amplitude of the fundamental harmonic of the back-EMF in the 60°TW-SPMSM is 3.6% higher than that of 30°TW-SPMSM, which verifies the correctness of previous analysis of no-load back-EMF. The total harmonic distortion (THD) of those are 8.17% and 6.69%, respectively. It can be seen that harmonics are relatively small in the two motors. The third harmonic in 60°TW-SPMSM is higher than that in 30° TW-SPMSM while the fifth, seventh and ninth harmonics in 30°TW-SPMSM are higher. The two machines produce a small seventh harmonic, reducing distortion in the back-EMF waveform [27].

4.2 | No-load air-gap magnetic density waveform

Table 3 presents the air-gap magnetic density characteristic of two studied six-phase PMSMs, predicted under no-load condition. It can be found that the air-gap magnetic density waveform of 60°TW-SPMSM is similar to that of 30°TW-SPMSM because they only differ in winding structure

Based on Fourier analysis, the air-gap magnetic density harmonic can be obtained, as shown in Table 3 and Figure 8. It can be noted that the peak value of the air-gap magnetic

TABLE 2 Back-electromotive force characteristic of two motors

Machines		60°TW-SPMSM	30°TW-SPMSM
Harmonic order	3	9.24%	6.43%
	5	0.48%	0.83%
	7	0.36%	0.61%
	9	0.16%	0.44%
Peak value		51.29 V	50.89 V
Fundamental harmonic		56.08 V	54.13 V
THD		8.17%	6.69%

Abbreviations: 30°TW-SPMSM, 30° phase-belt toroidal winding; 60°TW-SPMSM, 60° phase-belt toroidal winding configuration; THD, total harmonic distortion.

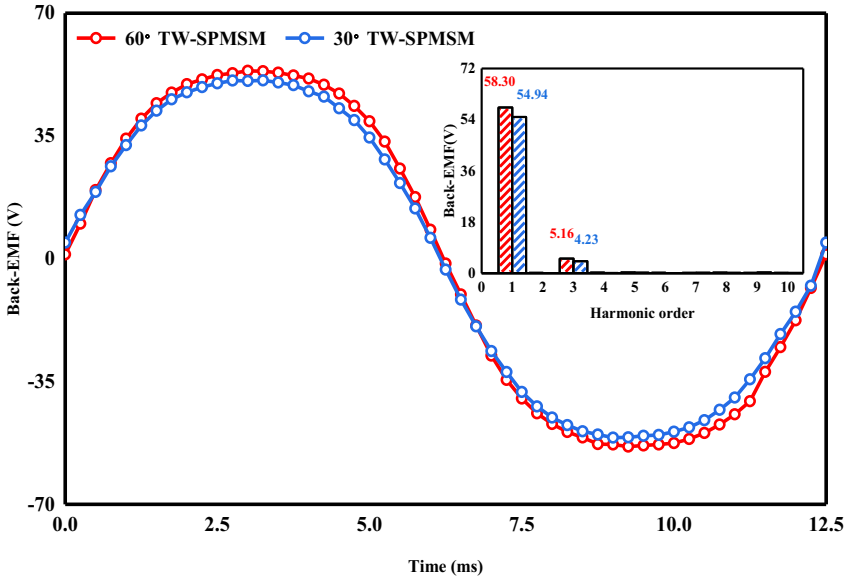

FIGURE 7 Back-electromotive force of two motors and its harmonic distribution under no load condition

density of the two motors are both 0.65 T. Meanwhile, the two motors have the same amplitudes of fundamental harmonic, which are both 0.77 T.

4.3 | Armature reaction field

The harmonic orders of armature reaction fields of two six-phase PMSMs are shown in Table 4. The minimum unit motor of the 60°TW-SPMSM consists of six coils and two poles while that of 30°TW-SPMSM contains 12 coils and two poles. Therefore, both minimum unit motors of the two motors can create armature reaction field of two poles. It can be noted that the peak value of 60°TW-SPMSM is 28.05 mT and the valley value is −27.98 mT in Figure 9. The armature reaction field characteristic of the 30°TW-SPMSM is shown in Figure 9. The peak value of 30°TW-SPMSM is 23.96 mT and the valley value is −23.64 mT. It can be seen that the fundamental harmonic is the main working armature reaction field harmonic of the 30°TW-SPMSM, which is 6.59% lower than that of 60°TW-SPMSM. In addition, the amplitudes of the fifth and seventh harmonics of 60°TW-SPMSM are significantly higher than those of 30°TW-SPMSM.

4.4 | Electromagnetic torque

Torque density of two motors can be compared through the comparison of electromagnetic torque since they have the same effective volume. The electromagnetic torque performance of two six-phase PMSMs at the same current (10 A) is shown in Figure 10 and Table 5.

It can be noted the average torque of the proposed 60° TW-SPMSM is larger than that of 30°TW-SPMSM at the same current (10A), which is 101.47% of the output torque of 30° TW-SPMSM. However, proposed 60°TW-SPMSM has larger torque ripple than 30°TW-SPMSM, which can reduce the overall performance of the motor.

The torque ripple can be expressed as follows:

$$T_{\text{ripple}} = \frac{T_{\max} - T_{\min}}{T_{\text{avg}}} \times 100\% \tag{11}$$

where $T_{\max}$ and $T_{\min}$ are maximum and minimum torque respectively, and T_{avg} is the average torque generated under load conditions.

Figure 11 shows the average torque versus currents from 0 to 10 A. It can be seen that the output torque increment of

TABLE 3 Comparison of air-gap magnetic density

Machines	60°TW-SPMSM	30°TW-SPMSM
Peak value (T)	0.65	0.65
Fundamental harmonic (T)	0.77	0.77
THD (%)	21.60	22.13

Abbreviations: 30°TW-SPMSM, 30° phase-belt toroidal winding; 60°TW-SPMSM, 60° phase-belt toroidal winding configuration.

TABLE 4 Armature reaction field characteristic of two motors

Machines	60°TW-SPMSM	30°TW-SPMSM
Peak value	28.07 mT	23.96 mT
Valley value	−27.99 mT	−23.64 mT
Fundamental harmonic	26.54 mT	25.35 mT

Abbreviations: 30°TW-SPMSM, 30° phase-belt toroidal winding; 60°TW-SPMSM, 60° phase-belt toroidal winding configuration; THD, total harmonic distortion.

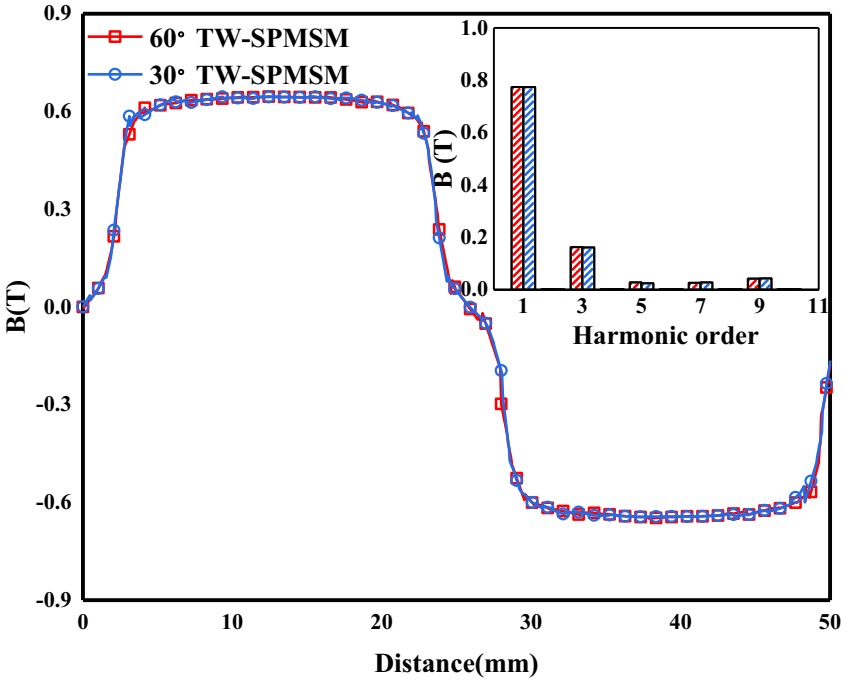

FIGURE 8 Air-gap magnetic density and its harmonic distribution of two motors

60°TW-SPMSM is almost the same as that of 30°TW-SPMSM. The output torque of two motors both increases relatively linearly with the increase of phase current, and the average torque of 30°TW-SPMSM is smaller than that of 60°TW-SPMSM. The torque coefficients of two motors are 5.73 and 5.63 Nm/A by curve fitting, respectively. When the current is 10 A, the average torque of 60°TW-SPMSM is 57.16 Nm, which is higher than that of 30°TW-SPMSM. The results show that the proposed 60°TW-SPMSM has a weak advantage in overload capacity.

4.5 | Torque-speed characteristic

In general, the torque-speed characteristics are divided into constant torque region and constant power region. To study the torque-speed characteristics of 60°TW-SPMSM and 30° TW-SPMSM, voltage source control is used to observe the change of average output torque by changing motor speed.

Figure 12 shows the torque–speed characteristic of two motors under load condition. Because the rated voltages of the two motors are the same, the inflection points of the torque–speed characteristic curve of the two motors are approximately the same. It can be seen that when the rotor speed is lower than 400 rpm, the output torque of the motors both are almost a constant value, and the working area of the motors is a constant torque area. When the motor speed increases, the voltage cannot increase when it is greater than the fundamental frequency. At this time, the output power is constant and the torque decreases with the increase of the motor speed. Moreover, because the torque difference between 30°TW-SPMSM and 60°TW-SPMSM is only 1.47%, the torque–speed characteristic curves of the two motors are approximately coincident.

4.6 | Efficiency of the motor

Motor loss usually includes copper loss and iron loss, which have a great influence on motor efficiency. For the six-phase PMSM, efficiency is an important performance index. Table 6 presents the losses and efficiency of two six-phase PMSMs, while ignoring mechanical loss.

The stator copper losses of two motors can be obtained by the Equations (12) and (13):

$$P_{cu} = nI^2R \tag{12}$$

$$R = \frac{2N_{Ph}l_{av}\rho}{100S} \tag{13}$$

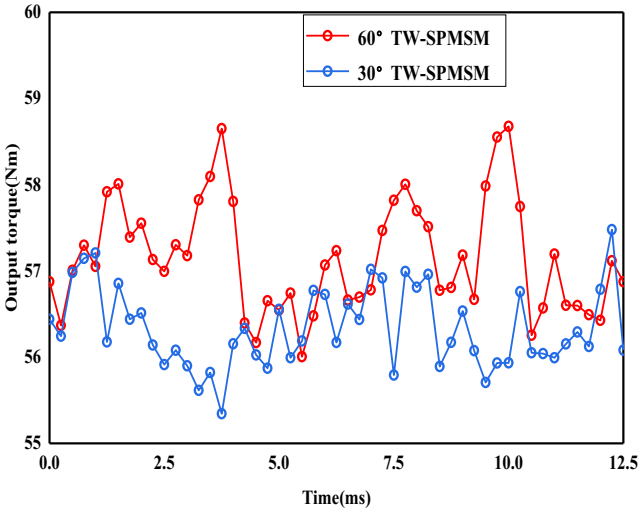

FIGURE 10 Torque waveform of the two motors at the same current (10A)

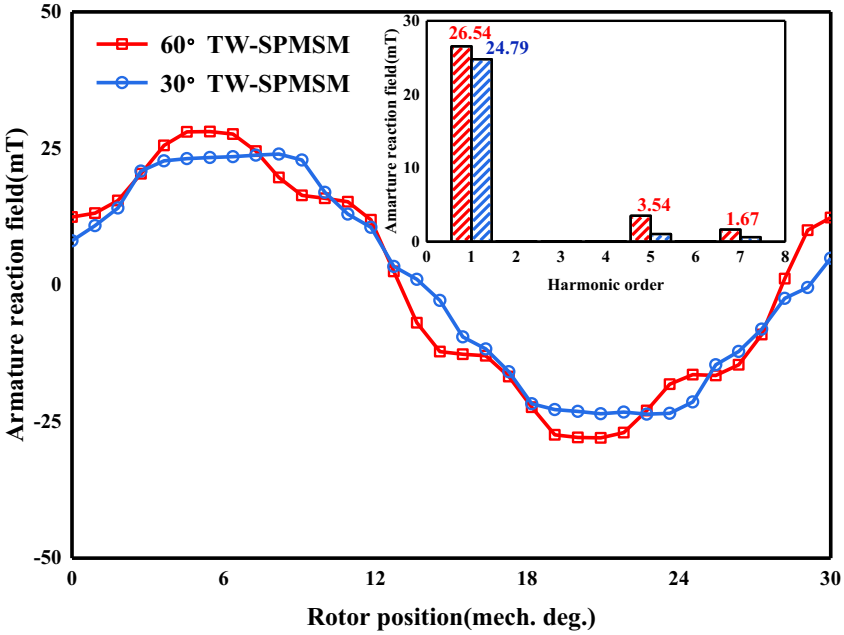

FIGURE 9 Armature reaction field and its harmonic distribution of two motors

where ρ is the resistivity of copper at 20°C, S is the sectional area of wire, and l_{av} is the length of half-turn armature winding.

Since the loss of electrical machinery is very small, it can be ignored that the motor efficiency η can be expressed as follows:

$$\eta = \frac{P_{out}}{P_{in}} = \frac{P_{out}}{P_{out} + P_{C_u} + P_{F_e}} . \quad (14)$$

The output power can be calculated by

$$P_{out} = T_{out}\Omega. \quad (15)$$

It can be noted that the output power of 30°TW-SPMSM is 1.45% lower than that of 60°TW-SPMSM. Since the total numbers of turns of two motors are the same, the copper loss of 60°TW-SPMSM is the same as that of 30°TW-SPMSM under the same current. The stator iron loss of 30°TW-SPMSM is 0.04 W smaller than that of 60°TW-SPMSM. Meanwhile, the efficiency of 30°TW-SPMSM is 0.18% smaller than that of the proposed 60°TW-SPMSM.

TABLE 5 Torque performance at the same current

Machines	60°TW-SPMSM	30°TW-SPMSM
Lower torque peak (Nm)	56.00	55.34
Higher torque peak (Nm)	58.68	57.48
Average torque (Nm)	57.16	56.33
Torque ripple (%)	4.69	3.80
Effective volume(L)	1.392	1.392
Torque density (Nm/L)	41.06	40.47

Abbreviations: 30°TW-SPMSM, 30° phase-belt toroidal winding; 60°TW-SPMSM, 60° phase-belt toroidal winding configuration.

5 | PROTOTYPE AND EXPERIMENTS

To indirectly validate the torque performance of the proposed 60°TW-SPMSM, the prototype of three-phase toroidal-winding machine which has the same main structure and composition as that of proposed motor was manufactured and shown in Figure 13.

As shown in Figure 13a, the toroidal windings are directly around the stator. The rotor with PM and motor assembly are shown in Figures 13b and d. The coil width is 12 mm as shown

TABLE 6 Losses and efficiency at the same current (10 A)

Items	60°TW-SPMSM	30°TW-SPMSM
Rated speed (rpm)	400	400
Average torque (Nm)	57.16	56.33
Output power (W)	2394.14	2359.37
Stator copper loss (W)	335.13	335.13
Stator iron loss (W)	3.01	2.97
Rotor loss (W)	1.00	0.98
Total loss (W)	339.14	339.08
Efficiency (%)	87.59	87.43

Abbreviations: 30°TW-SPMSM, 30° phase-belt toroidal winding; 60°TW-SPMSM, 60° phase-belt toroidal winding configuration.

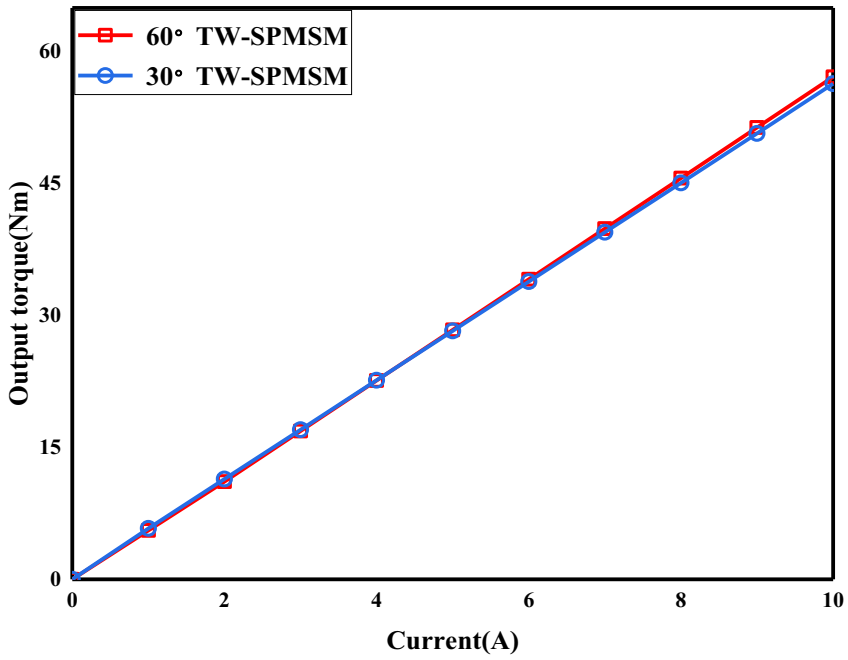

FIGURE 11 Torque-current curves of two analysed permanent magnet synchronous motor (PMSM) machines

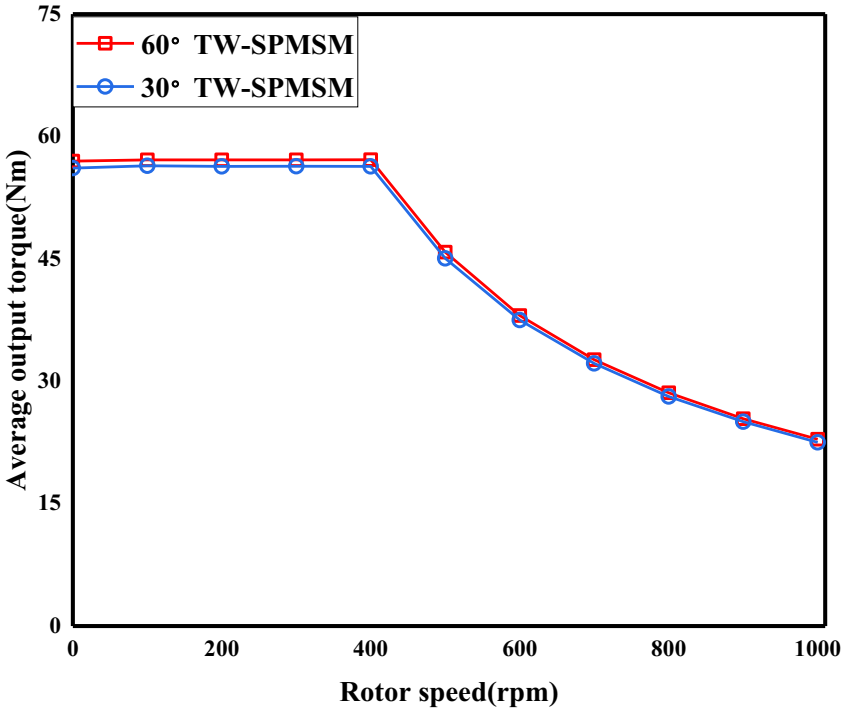

FIGURE 12 Torque–speed characteristic of two motors under load condition

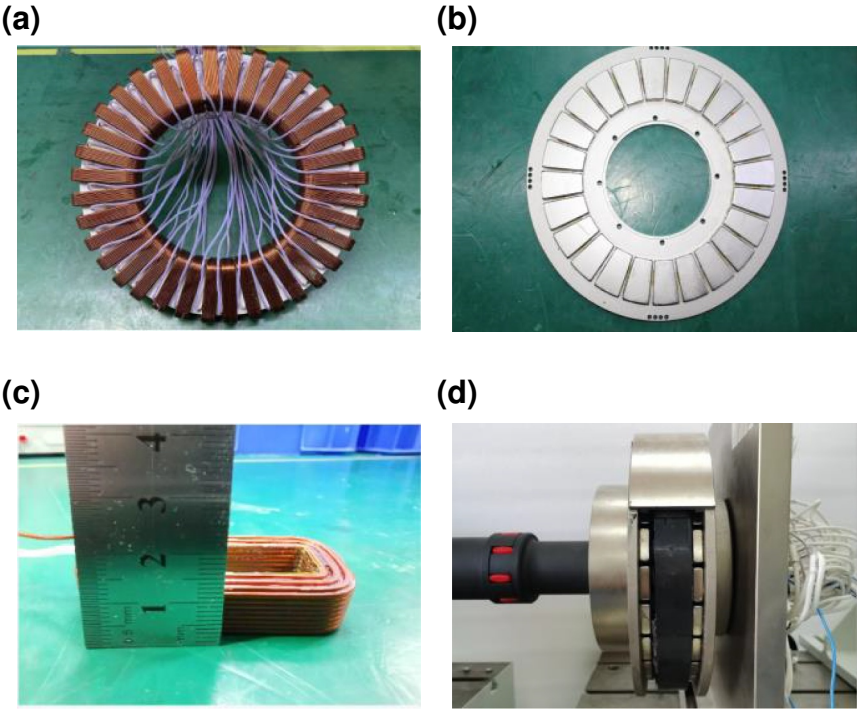

FIGURE 13 Prototype of the three-phase PMSM machine. (a) Stator. (b) Assembled rotor. (c) Toroidal winding. (d) Motor assembly

in Figure 13c. The experimental platform of the prototype is shown in Figure 14, which includes load motor, torque transducer and the prototype of the three-phase toroidal-winding motor.

According to the parameters of the three-phase toroidal-winding prototype, two finite-element models of three-phase PMSMs with 120° phase-belt toroidal winding (120° TWPMSM) and traditional toroidal winding (TTWPMSM) are established. The two motors only differ in winding structure.

The no-load back-EMF of the two motors at rated speed (400 rpm) is shown in Figure 15. It can be seen that the peak value of no-load back-EMF of 120°TWPMSM is 11.42% higher than that of TTWPMSM.

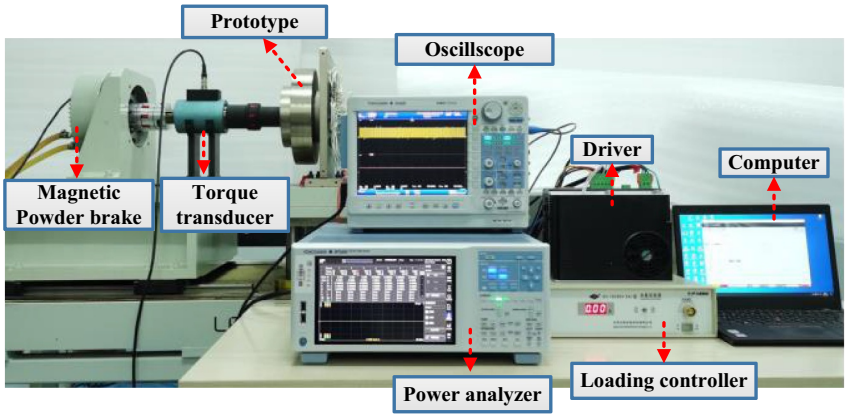

FIGURE 14 The experimental platform of the prototype

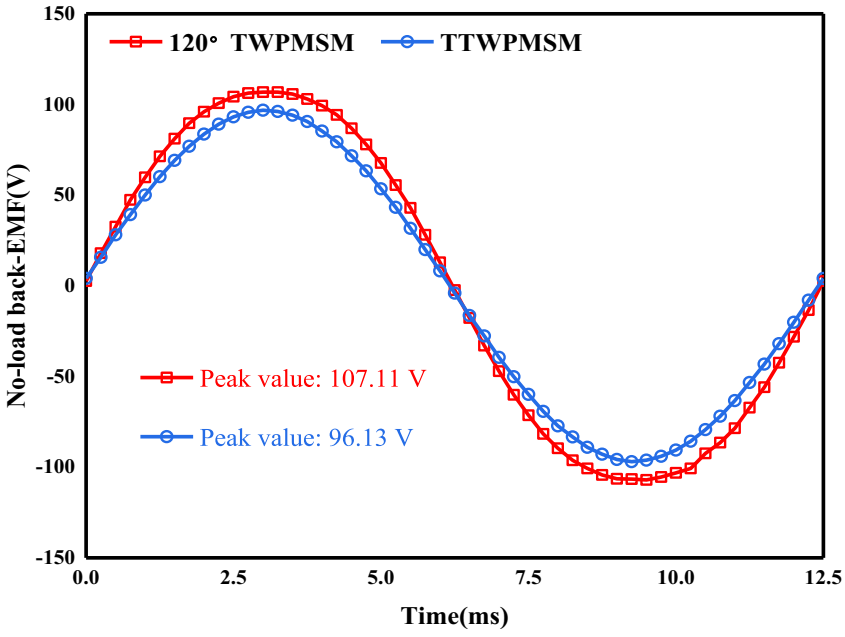

FIGURE 15 No-load back-electromotive force of 2 three-phase motors

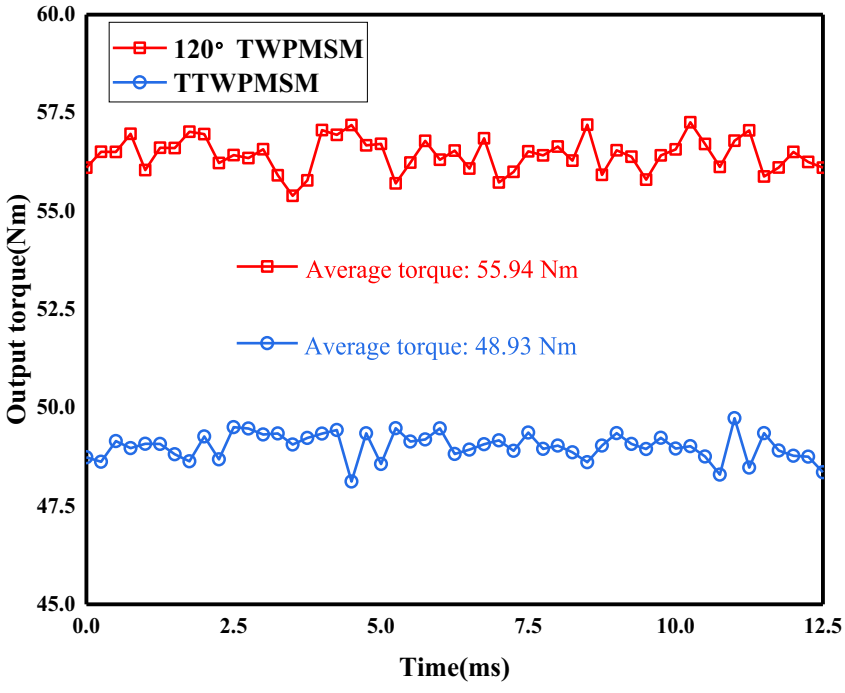

FIGURE 16 Output torque of two motors under load condition of 10 A phase current

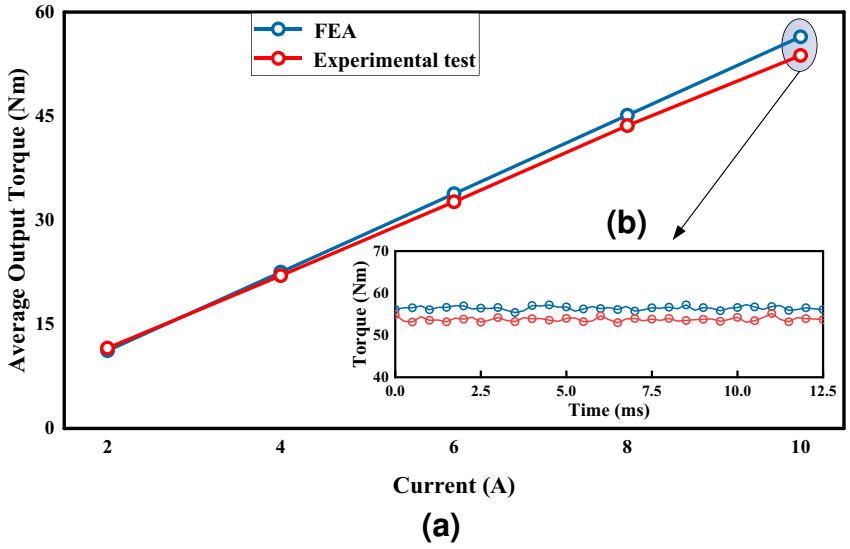

FIGURE 17 Measured and predicted output torque. (a) Output torque versus current. (b) Output torque under load condition of 10 A phase current

Output torque waveforms of two motors under load condition of 10 A phase current are shown in Figure 16. It can be noted that the average output torque of 120°TWPMSM is increased by 14.33% compared with that of TTWPMSM. This proves that the 120°TWPMSM can not only produce rotating magnetic field, but also improve the torque density of the motor.

In order to verify the finite-element analysis of 120° TWPMSM, experimental tests are carried out on the prototype. Figure 17a shows the measured output torque versus current. It can be noted that the measured output torque increases relatively linearly with the rise of current, which agrees well with finite-element analysis. It can be found that the deviation of torque becomes larger with higher current. But the calculated output torque is higher than the measured torque. The 3D finite-element simulated and measured output torque at the same current (10 A) of 120°TWPMSM machine is shown in Figure 17b. It can be seen that the measured output torque has similar torque ripple with the calculated results. Meanwhile, the result of finite-element simulated is still higher than the measured output torque.

Due to the machining accuracy, the air gap of the prototype is 0.5 mm larger than that of the 3D finite-element model, which leads to the difference of 4.76% between the torque measured by the prototype experiment and the torque obtained by the finite-element simulation under the load condition of 10 A phase current. Despite the shortage of the manufacturing technology which leads to variation in the results of simulation and measured results, it can be seen that the torque performance of prototype is basically the same as that of the finite-element model.

Figure 18 shows the no-load line to line back-EMF of the prototype of three-phase PMSM machine. It can be found that the peak value of the no-load line to line back-EMF of the experimental test and FEA is 187.68 and 192.94 V, respectively. The error between the simulation data and the experimental data is 2.8%, which verifies the consistency and scientificity of the results between the prototype and the finite-element model.

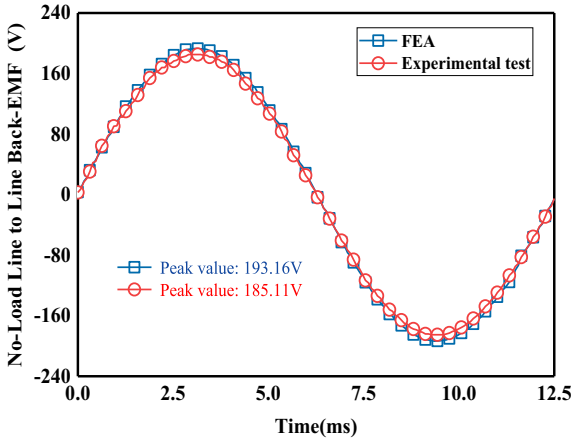

FIGURE 18 No-load line to line back-electromotive force of prototype of three-phase PMSM machine

In conclusion, the three-phase toroidal winding motor prototype experiments verify the consistency of the FEA results and experimental results. This proves that it is feasible to analyse the motor by this method. As the proposed 60°TWSPMSM motor is a special dual three phase motor composed of two 120°TWPMSMs, the consistency of the experimental and simulation results of the two three-phase motors can indirectly prove the scientificity of the proposed six-phase motor. Meanwhile, based on the results of 120°TWPMSM, the simulation results of six-phase motor can be reasonably predicted to be consistent with the experimental results of its prototype.

6 | CONCLUSION

In this study, a six-phase axial-flux PMSM with 60° phase-belt toroidal winding configuration is presented and analysed. The structure and operation principle of the proposed motor was

introduced. Furthermore, a comparative study of air-gap magnetic density and phase back-EMF under the no-load condition of 60°TW-SPMSM and 30°TW-SPMSM is reported. The armature reaction field, torque density, efficiency and torque-speed characteristic under load condition of two motors are compared. The comparison results show the reasonability of the 60°TW-SPMSM and validate the propitious torque density of the proposed 60°TW-SPMSM. Last, the experimental test results of three-phase PMSM with 120° phase-belt toroidal winding further indirectly prove the scientificity of the proposed motor finite-element model. The findings can be concluded as below:

(i) Based on the same effective volume and rotor speed, the fundamental component of no-load back-EMF of proposed 60°TW-SPMSM is 3.6% higher than that of 30° TW-SPMSM.
(ii) Under the same current, the output torque of the proposed machine is larger than that of 30°TW-SPMSM. However, the torque ripple of the proposed motor is larger than that of the motor with 30° phase-belt toroidal winding. In addition, the torque coefficients of two motors are 5.73 and 5.63 Nm/A through curve fitting. It can be noted that the proposed motor has better torque density.
(iii) Although the output power of the six-phase PMSM with 30° phase-belt toroidal winding is lower than that of the proposed motor under the same load condition, the copper loss caused of the proposed motor is higher. Thus, there is no appreciable increase in efficiency.
(iv) When the motor runs at low rotor speed, the output torque is approximately constant. When the rotor speed increases greater than the rated speed (400 rpm), the output power remains constant due to the limitation of voltage. The output torque decreases with the increase of rotor speed.

The proposed 60°TW-SPMSM gets higher torque density due to its 60° phase-belt toroidal winding. Moreover, its slotless structure eliminates the cogging torque. This provides a new thinking of improving torque density.

ACKNOWLEDGEMENT

The authors would like to thank the members of the research group for providing many technical advices in support of this research, and Shu-hua Wang and the Yokokawa Robot (Shenzhen) Co., Ltd for technical support. This work is partially supported by the Natural Science Foundation of China under grant No.51,777,060, the China Postdoctoral Science Foundation (2020M682342), in part by the Major Special Project for Collaborative Innovation in Zhengzhou No. 20XTZX12023. Shu-hua Wang and the Yokokawa Robot (Shenzhen) Co., Ltd provide technical support in support of this research.

CONFLICT OF INTEREST

Authors have no conflict of interest to declare.

PERMISSION TO REPRODUCE MATERIALS FROM OTHER SOURCES

None.

DATA AVAILABILITY STATEMENT

Research data are not shared.

ORCID

Jikai Si https://orcid.org/0000-0002-9663-2349
Yihua Hu https://orcid.org/0000-0002-1007-1617

REFERENCES

1. Xu, Y., et al.: Comparisons of Concentrated Fractional Winding and Distributed Winding of Permanent Magnet Synchronous Motors for Biped Robot. 2019 22nd International Conference on Electrical Machines and Systems (ICEMS), pp. 1–4. IEEE (2019)
2. Wang, W., et al.: Fault-tolerant control of dual three-phase permanent-magnet synchronous machine drives under open-phase faults. IEEE Trans. Power Electron. 32(3), 2052–2063 (2017)
3. Wu, Z., et al.: Comparison and analysis of permanent magnet vernier motors for low-noise in-wheel motor application. IET Electr. Power Appl. 14(2), 274–281 (2020)
4. Akune, R., et al.: Study of High Torque Density Interior Permanent Magnet Synchronous Motor with Flexible Orientation Nd2Fe14B Sintered Magnet. 2016 XXII International Conference on Electrical Machines and Systems (ICEMS), pp. 578–584. IEEE (2016)
5. Du, Z.S., Lipo, T.A.: High Torque Density Ferrite Permanent Magnet Vernier Motor Analysis and Design with Demagnetization Consideration, pp. 6082–6089. IEEE Energy Conversion Congress and Exposition (2015)
6. Parsapour, A., et al.: High Torque Density Double Stator Permanent Magnet Electric Machine, pp. 664–670. IEEE International Electric Machines & Drives Conference (IEMDC) (2019)
7. Ullah, W., et al.: Torque characteristics of high torque density partitioned pm consequent pole flux switching machines with flux barriers. CES Trans. On Electr. Machines And system. 4(2), 130–141 (2020)
8. Lindh, P., et al.: Direct liquid cooling method verified with a permanent-magnet traction motor in a bus. XIII International Conference on Electrical Machines, pp. 2472–2477. ICEM (2018)
9. Parsa, L., Toliyat, H.A.: Five-phase permanent-magnet motor drives. IEEE Trans. Ind. Appl. 41(1), 30–37 (2005)
10. Lyra, R.O.C., Lipo, T.A.: Torque density improvement in a six-phase introduction motor with third harmonic current injection. IEEE Trans. Ind. Appl. 38(5), 1351–1360 (2002)
11. Liu, Y., Zhu, Z.Q.: Electromagnetic Performance Comparison of 18-Slot/26-Pole and 18-Slot/10-Pole Fractional Slot Permanent Magnet Surface-Mounted Machines. 2017 20th International Conference on Electrical Machines and Systems (ICEMS), pp. 1–6. IEEE (2017)
12. Rahman, K.M., et al.: Application of direct-drive wheel motor for fuel cell electric and hybrid electric vehicle propulsion system. IEEE Trans. Ind. Appl. 42(5), 1185–1192 (2006)
13. El-Refaie, A.M.: Fractional-slot concentrated-windings synchronous permanent magnet machines: opportunities and challenges. IEEE Trans. Ind. Electron. 57(1), 107–121 (2010)
14. Choe, Y., et al.: Comparison of concentrated and distributed winding in an IPMSM for vehicle traction. International Conference on Advances in Energy Engineering, pp. 1368–1373. Bangkok, Thailand (2011)
15. Li, H., Zhu, Z.Q., Hua, H.: Comparative analysis of flux reversal permanent magnet machines with toroidal and concentrated windings. IEEE Trans. Ind. Electron, 5278–5290 (2019)
16. Wei, Y., et al.: Design and characteristic analysis of a six-phase direct-drive permanent magnet synchronous motor with 60° phase-belt toroidal winding configuration for electric vehicle. IET Electr. Power Appl. pp. 1–8 (2020)

17. Potgieter, J.H.J., Kamper, M.J.: Double PM-rotor, toothed, toroidal-winding wind generator: a comparison with conventional winding direct-drive PM wind generators over a wide power range. IEEE Trans. Ind. Appl. 52(4), 2881–2891 (2016)
18. Li, D., et al.: Consequent-pole toroidal-winding outer-rotor vernier permanent-magnet machines. IEEE Trans. Ind. Appl. 51(6), 4470–4481 (2015)
19. Gao, C., et al.: A novel direct-drive permanent magnet synchronous motor with toroidal windings. Energies. 12(3), 1–12 (2019)
20. Jin, F., et al.: Analysis of a Six-Phase Direct-Drive Permanent Magnet Synchronous Motor with Novel Toroidal Wingdings. 2019 IEEE Vehicle Power and Propulsion Conference (VPPC), pp. 1–6. IEEE (2019)
21. Geng, W., Zhang, Z., Li, Q.: High torque density fractional-slot concentrated-winding axial-flux permanent-magnet machine with modular SMC stator. 2019 IEEE Energy Conversion Congress and Exposition (ECCE). pp. 2991–2995. IEEE (2019)
22. Hultman, L.O., Jack, A.G.: Soft magnetic composites-materials and applications. IEEE Int. Elect. Mach. Drives Conf. 516–522 (2003)
23. Wanjiku, J., et al.: Influence of slot openings and tooth profile on cogging torque in axial-flux PM machines. IEEE Trans. Ind. Electron. 63(12), 7578–7589 (2015)
24. Huang, S.D., et al.: Design and characteristic analysis of an axial-flux permanent magnet synchronous motor with contra-rotating rotors. Trans. China Electrotech. Soc. 32(23), 72–80 (2017)
25. Huang, S., et al.: A comparison of power density for axial flux machines based on general purpose sizing equations. IEEE Trans. Energy Convers. 14(2), 185–192 (1999)
26. Sun, M.C., et al.: Analysis of open circuit back electromotive force in slotless toroidal type winding axial flux permanent magnet machine. Electr. Mach. & Control Appl. 44(9), 1–8 (2017)
27. Zhu, Z., et al.: Comparative study of the electromagnetic performance of switched flux permanent magnet machines. IET Electr Power Appl. 9(4), 297–306 (2015)

How to cite this article: Si, J., et al.: A novel high torque density six-phase axial-flux permanent magnet synchronous motor with 60° phase-belt toroidal winding configuration. IET Electr. Power Appl. 16(1), 41–54 (2022). https://doi.org/10.1049/elp2.12133